



Contents lists available at ScienceDirect

Spectrochimica Acta Part A: Molecular and Biomolecular Spectroscopy

journal homepage: www.elsevier.com/locate/saa

Substitution effect on luminescent property of thermally activated delayed fluorescence molecule with aggregation induced emission: A QM/MM study

Qi Lu, Guanyu Jiang, Feiyan Li, Lili Lin, Chuan-Kui Wang, Jianzhong Fan^{*}, Yuzhi Song^{*}

Shandong Province Key Laboratory of Medical Physics and Image Processing Technology, School of Physics and Electronics, Shandong Normal University, Jinan 250358, China

ARTICLE INFO

Article history:

Received 3 September 2019

Received in revised form 25 November 2019

Accepted 14 December 2019

Available online 19 December 2019

Keywords:

Thermally activated delayed fluorescence

Aggregation induced emission

Substitution effect

QM/MM method

ABSTRACT

Pure organic molecules with blue emission have attracted much attention due to its important application in organic light emitting diodes (OLEDs), especially for which with aggregation induced emission (AIE) and thermally activated delayed fluorescence (TADF) properties. Theoretical study to reveal the inner luminescent mechanisms can promote its development. In this work, four kinds of molecules with perfluorobiphenyl (PFBP) unit as acceptor, non-substituted and tert-butyl substituted 9,9-dimethyl-9,10-dihydro-acridine (DMAC) unit as donors, are selected and their photophysical properties are studied in detail. The surrounding environment effects in toluene and solid phase are taken into consideration by the polarized continuum model (PCM) and the combined quantum mechanics and molecular mechanics (QM/MM) method respectively. Results show that geometric changes between the first singlet excited state (S_1) and ground state (S_0) are restricted in solid phase with decreased root-mean squared displacement (RMSD). Moreover, the Huang-Rhys factors and reorganization energies we calculated are all decreased in solid phase, which indicates that the non-radiative energy consumption process of S_1 is hindered by enhanced intermolecular interactions in rigid environment, and it brings aggregation induced emission phenomenon. Furthermore, the substitution effect of tert-butyl in donor unit can efficiently decrease the energy gap and increase the spin-orbit coupling (SOC) constant, further promotes the intersystem crossing (ISC) and reverse intersystem crossing (RISC) rates. Meanwhile, molecules with donor-acceptor-donor (D-A-D) configuration have more efficient luminous performance than D-A type molecules due to the enhanced ISC and RISC processes. Thus, tert-butyl substituted D-A-D type molecules have outstanding TADF features. Our investigations provide a theoretical perspective for AIE and TADF mechanisms and propose a design strategy for efficient TADF molecules, which could promote the development of OLEDs.

© 2019 Elsevier B.V. All rights reserved.

1. Introduction

Thermally activated delayed fluorescence (TADF) which known as E-type fluorescence, has attracted much attention due to its high utilization of both singlet and triplet excitons in organic light emitting diodes (OLEDs) [1]. For the electroluminescence process, the generation ratio of singlet and triplet excitons is 1:3 [2–4]. Thus, it is of great importance to improve the utilization of triplet excitons. In 2012, Adachi's group found that unlike traditional fluorescence and phosphorescence, molecules with TADF phenomenon can make full use of the singlet and triplet excitons by a fast reversed intersystem crossing (RISC) process. As we all know, the efficient RISC process is related to the energy gap (ΔE_{st}) between the lowest singlet excited state (S_1) and the lowest triplet excited state (T_1) with a non-vanishing spin-orbital coupling (SOC). One of the most effective ways to decrease the S_1 - T_1 energy gap is

constructing D-A type molecules by connecting electron-donating (D) groups and electron-accepting (A) groups with a large torsion angle between them [5–9]. The above mentioned strategy can effectively separate the spatial overlap between the highest occupied molecular orbital (HOMO) and the lowest unoccupied molecular orbital (LUMO). Thus, a small ΔE_{st} can be obtained. However, the structural changes, strength and TADF efficiency of D-A type molecules also depend on the environment, temperature, external force, and bonding mode, etc. [10–12]. Thus, theoretical investigations to reveal the relationship between molecular geometry and TADF properties are important for developing new efficient emitter in OLEDs [13]. Furthermore, the majority of organic emitters suffer from aggregation-caused quenching (ACQ) and exciton quenching effects, which extremely hinders the stability and fabrication of devices and affects the practical applications [14]. Fortunately, Tang et al. discovered the molecules that aggregate to induce luminescence, namely, aggregation induced emission (AIE) phenomenon [15,16]. AIE materials can be applied in many fields, such as biology, physics, and chemistry, etc. The use of molecules

^{*} Corresponding author.E-mail addresses: fanjianzhongvip@163.com (J. Fan), yzsong@sdu.edu.cn (Y. Song).

with AIE property verified that the device can be effectively increased luminous efficiency and stability. TADF molecules with AIE feature are characterized by low cost, high efficiency and long lifetime, and AIE-TADF molecules show the wide application in OLEDs [17]. Through the detailed study of TADF properties in solid phase, it was found that the existence of AIE effect was confirmed by restricted intramolecular rotation-limiting molecules in the form of non-radiative transition. Moreover, monochromatic emitters can produce chromatic aberrations, it usually caused by intramolecular or intermolecular interactions such as π - π stacking, hydrogen bonding, and conformational changes, thus TADF molecules with discoloration properties can be studied based on these characteristics [18]. In current studies, the luminous efficiency of multi-color TADF molecules is still very low, so clear theoretical design strategies to develop more efficient TADF molecules are expected [19,20]. Recently, Hladka's group synthesized the blue-emitting molecules which used 9,9-dimethyl-9,10-dihydro-acridine (DMAC) as donor and perfluorobiphenyl (PFBP) as acceptor, which possesses both TADF and AIE properties [2]. In this work, four kinds of blue emitting TADF molecules (denoted as PFBP-1a, PFBP-1b, PFBP-2a, and PFBP-2b) are studied with geometry changes from D-A to D-A-D configuration and tert-butyl substitution in DMAC unit (shown in Fig. 1). TADF and AIE properties of different types of molecules are revealed. The solution effect in toluene is considered by polarized continuum model (PCM) [21,22]. Moreover, the quantum mechanics and molecular mechanics (QM/MM) method is used to simulate molecules in solid phase [23–26]. The radiative and non-radiative energy consumption processes are studied by Einstein's spontaneous emission equation and thermal vibration correction function (TVCF) method respectively. Moreover, the ISC and RISC rates are calculated by the Marcus equation. Thus, the AIE-TADF property in solid phase is revealed.

2. Theoretical method

in order to study the effects of molecular configuration of D-A and D-A-D on TADF properties, the excited state properties are studied by time-dependent density functional theory (TD-DFT) [27]. The specific

luminescent physical properties can be measured by different rate parameters. When calculating the processes S_1 and S_0 states, the radiative decay rate k_r and non-radiative decay rate k_{nr} are required. Radiative decay rate k_r is calculated by Einstein spontaneous emission equation with the consideration of refractive index of the medium, and it can be written as

$$k_r = \frac{f \Delta E_{fi}^2}{1.499} n^2 \quad (1)$$

where f is oscillator strength, ΔE_{fi} is the vertical emission energy and n represents the refractive index of the medium. Here, the value of n for toluene is set as 1.496. More details can be found in reference [28,29].

As for non-radiative decay rate k_{nr} , it is calculated by first-order perturbation theory and Fermi's golden rule (FGR).

$$k_{nr} = \frac{2\pi}{\hbar^2} \sum_{u,v} P_{iv} |H_{fu,iv}|^2 \delta(E_{iv} - E_{fu}) \quad (2)$$

Here P_{iv} is Boltzmann distribution function of the initial state and H is the interaction between two different Born-Oppenheimer states, which includes two components,

$$\hat{H}\Psi_{iv} = \hat{H}^{BO} \Phi_i(r, Q) \Theta_{iv}(Q) + \hat{H}^{SO} \Phi_i(r, Q) \Theta_{iv}(Q) \quad (3)$$

\hat{H}^{BO} is the nonadiabatic coupling and \hat{H}^{SO} is the spin-orbit coupling (SOC). The non-radiative decay rate from S_1 to S_0 is written as

$$k_{nr} = \frac{2\pi}{\hbar} \sum_{kl} R_{kl} Z_i^{-1} \sum_{vu} v_{iu} e^{-\beta E_{iv}} \langle \Theta_{fu} | \hat{P}_{fk} | \Theta_{iv} \rangle \langle \Theta_{iv} | \hat{P}_{fl} | \Theta_{fu} \rangle \delta(E_{iv} - E_{fu}) \quad (4)$$

Here, $R_{kl} = \langle \Phi_f | \hat{P}_{fk} | \Phi_i \rangle \langle \Phi_i | \hat{P}_{fl} | \Phi_f \rangle$ is the nonadiabatic electronic coupling.

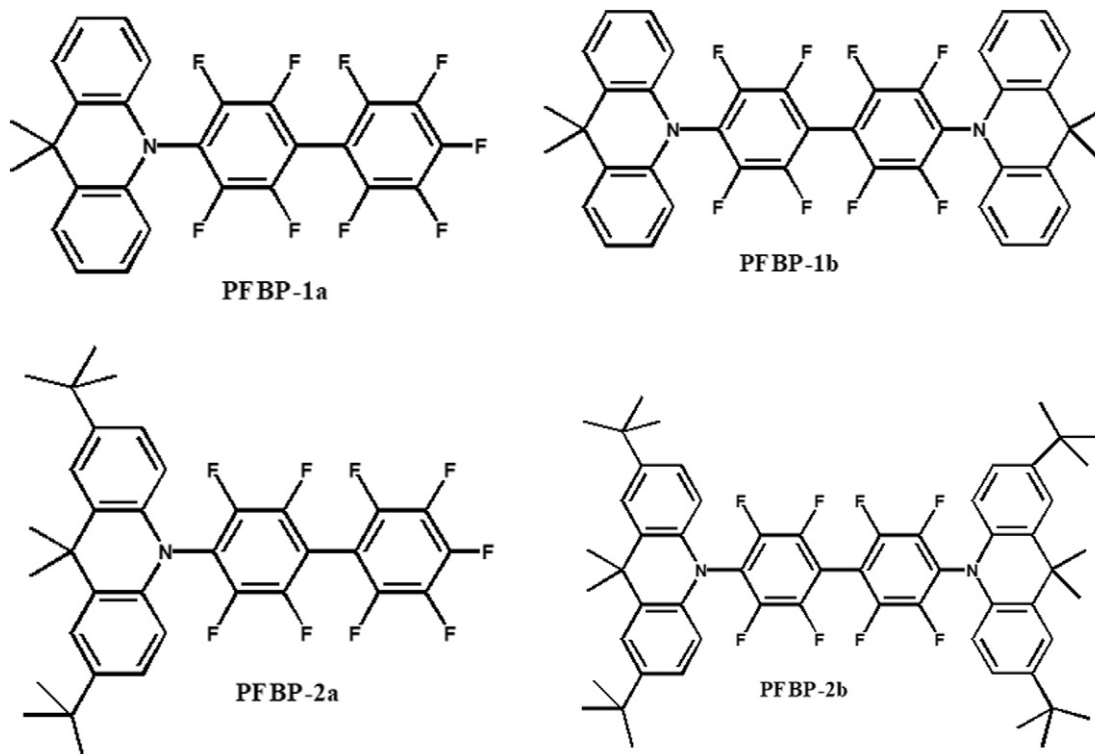


Fig. 1. Molecular configuration of PFBP-1a, PFBP-1b, PFBP-2a and PFBP-2b.

$\hat{p}_{jk} = -i\hbar \frac{\partial}{\partial Q_{jk}}$ is the normal momentum operator of the k th normal mode in the final electronic state. Z_i is the partition function. By employing the Franck-Condon principle and Fourier transform of the delta function, Eq. (4) can be expressed as

$$k_{nr} = \sum_{kl} \frac{1}{\hbar^2} R_{kl} \int_{-\infty}^{\infty} dt \left[e^{i\omega_{ij}t} Z_i^{-1} \rho_{ic,kl}(t, T) \right] \quad (5)$$

where $\rho_{ic}(t, T)$ is the TVCF.

Moreover, the ISC and RISC rates between singlet and triplet states can be calculated by utilizing the classical Marcus rate equation,

$$K_{ji} = \frac{V_{ji}^2}{\hbar} \sqrt{\frac{\pi}{K_B T \lambda}} \exp \left[-\frac{(\Delta G_{ji} + \lambda)^2}{4\lambda K_B T} \right] = \frac{V_{ji}^2}{\hbar} \sqrt{\frac{\pi}{K_B T \lambda}} \exp \left[-\frac{\Delta G_{ji}^{\ddagger}}{K_B T} \right] \quad (6)$$

where K_B is the Boltzmann constant, T the temperature of 300 K, and V_{ji} the spin-orbit coupling between S_1 and T_1 states. V_{ji} can be calculated by using the quadratic response function method, which is implemented in

the Dalton program [30]. In Eq. (6), $\Delta G_{ji}^{\ddagger} = \frac{(\Delta G_{ji} + \lambda)^2}{4\lambda}$, where ΔG_{ji} is the energy difference between the S_1 and T_1 states, and λ is the corresponding reorganization [31–33]. In calculation of the ISC rate, $\Delta G_{ji} = E_{S_1} - E_{T_1}$, and $\Delta G_{ji} = E_{T_1} - E_{S_1}$ for the reverse RISC process. In our calculation, the reorganization energy λ is obtained by four-point calculations according to the adiabatic potential energy surface. $E(T_1 @ S_1)$ represents the energy of the triplet state at the singlet geometry, $E(S_1 @ T_1)$ is the energy of the singlet state at the triplet geometry, $E(T_1)$ is the minimum energy in T_1 surface and $E(S_1)$ is the minimum energy in S_1 surface. Thus, the reorganization energy can be calculated as follows

$$\lambda = \{E(T_1 @ S_1) - E(T_1)\} + \{E(S_1 @ T_1) - E(S_1)\}$$

Moreover, based on the Marcus equation, the ISC rate is calculated with $\lambda_{ISC} = E(T_1 @ S_1) - E(T_1)$. While for calculating the RISC rate, the energy is set as $\lambda_{RISC} = E(S_1 @ T_1) - E(S_1)$ [34,35]. All above mentioned methodologies and applications of these functions are illustrated in detail in Peng's and Shuai's previous works [36–40].

3. Computational approach

In the calculation, density functional theory (DFT) is used to optimize the geometric structure of ground state molecules, while time-dependent density functional theory (TDDFT) is used to optimize the geometry of excited states [41]. It is determined that the appropriate functional is closely related to the study of the properties of excited states. Thus, several functions including B3LYP [42], BMK [43], PBE0 [44], and M06-2X [45] are tested for PFBP-1a, PFBP-1b, PFBP-2a and PFBP-2b respectively. The emission wavelengths we calculated are collected in Table 1. By comparing the wavelength and adiabatic energy with the experimental value, the functional of BMK with 6-31 g (d) [46] basis set is determined. For molecule in toluene, the surrounding environment is simulated by PCM method with the chosen functional BMK and 6-31g (d) basis set. Moreover, after the geometry optimizations of ground and excited states, corresponding frequency

calculations are performed. Since no imaginary frequency is found, the optimized ground and excited state geometries represent the true minimum on respective potential energy surfaces. Specifically, the equilibrium solvation method is employed in both geometry optimization and vibrational frequency calculation for singlet and triplet states involved in this paper. The nonequilibrium solvation method is used to obtain the vertical transition energies for both singlet and triplet states. As for molecule in solid phase, we perform calculations by QM/MM with two-layer ONIOM approach based on the X-crystal data and corresponding data are shown in Fig. 2 [47,48]. The central molecule is regarded as high layer, calculated by QM method. Meanwhile the surrounding molecules are regarded as low layer and calculated by MM method [49]. Moreover, the universal force field (UFF) is adopted for the MM part and the electronic embedding is selected in our QM/MM calculations. In addition, molecules of MM part are frozen during the QM/MM geometry optimizations for S_0 , S_1 and T_1 states. All these calculations are performed in Gaussian 16 package [50]. Furthermore, we use the Marcus equation to calculate the ISC and RISC rates. Meanwhile, the

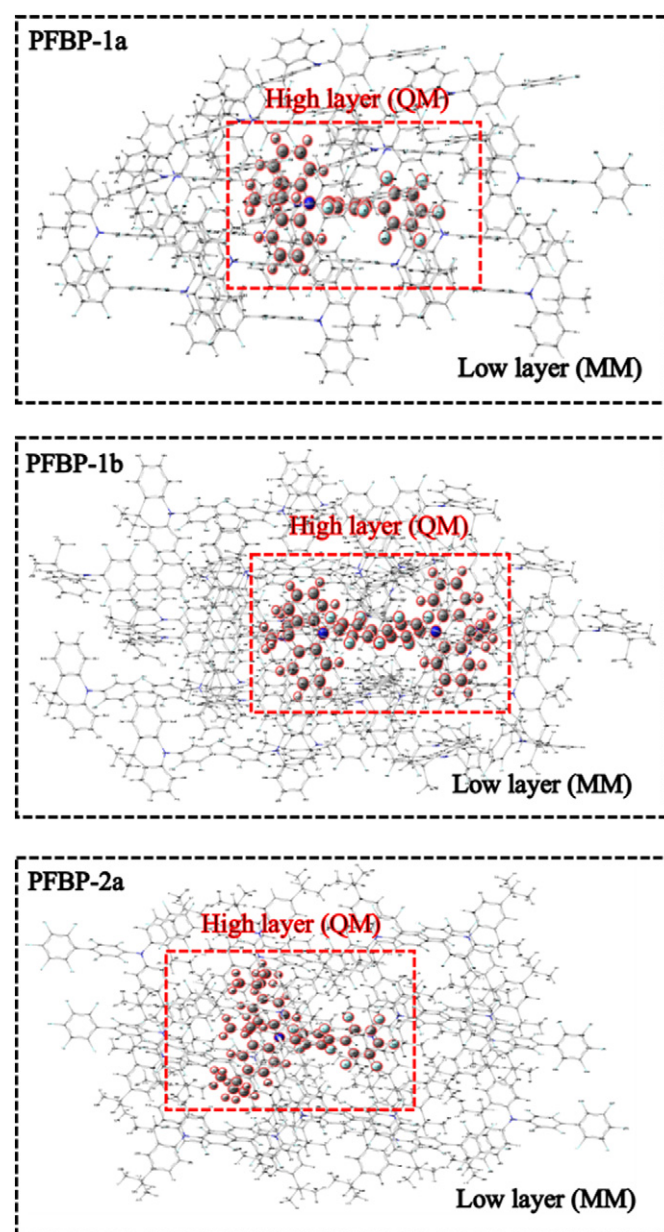


Fig. 2. ONIOM model: the centered PFBP-1a, PFBP-1b, PFBP-2a is treated as the high layer and the surrounding molecules are regarded as the low layer.

Table 1

The calculated emission wavelengths by different functional and the experimental data are listed for comparison.

	HF%	PFBP-1a	PFBP-1b	PFBP-2a	PFBP-2b
B3LYP	20%	605nm	575 nm	636 nm	–
PBE0	25%	565 nm	542 nm	594 nm	–
BMK	42%	503 nm	503 nm	535 nm	527 nm
M062X	54%	478 nm	473 nm	495 nm	–
Exp ^a		493 nm	497 nm	528 nm	516 nm

^a Experimental data.

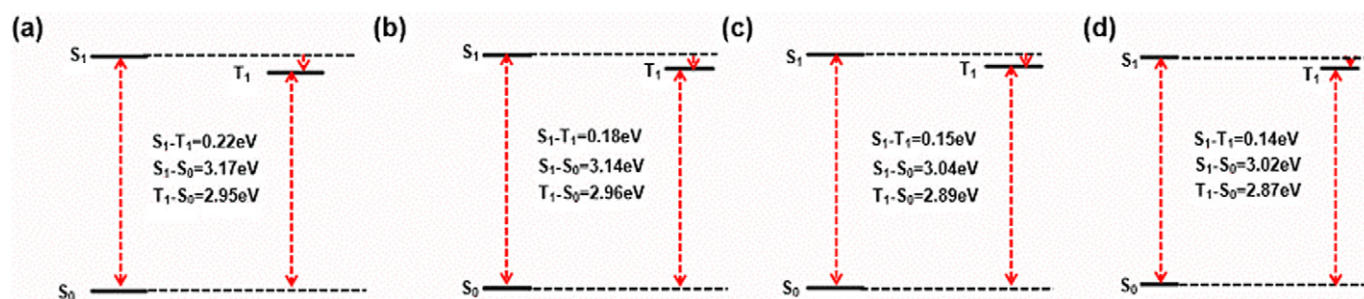


Fig. 3. Energy gap in liquid phase for PFBP-1a (a), PFBP-1b (b), PFBP-2a (c), PFBP-2b (d).

luminous properties of the four molecules either in toluene or in solid phase are studied by MOMAP (Molecular Materials Property Prediction Package) [36]. At the same time, the Huang-Rhys factor and recombination energy which can be used to measure the non-radiative energy consumption processes are calculated by DUSHIIN program and the reorganization energies can be projected on internal coordinates following Reimers' algorithm [51].

4. Results and discussion

4.1. Effect of D-A-D structure on luminescence properties

In this section, the effects of molecular configuration of D-A and D-A-D on TADF properties are studied. Firstly, based on the determined functional of BMK and 6-31 g (d) basis set, the energy landscapes for all molecules in toluene and solid phase are calculated for ground state and excited state by DFT and TDDFT method respectively. Corresponding results are gathered in Figs. 3 and 4. In the liquid phase, the adiabatic energy gap between S_1 and T_1 is 0.22 eV for PFBP-1a which possesses D-A structure, and it reduced to 0.18 eV for PFBP-1b (b) which possesses D-A-D structure. A similar result can be found by comparing the data of PFBP-2a with PFBP-2b. As for in solid phase, the S_1-T_1 gap of PFBP-1b is also decreased compared with that of PFBP-1a. This shows that the adiabatic energy gap can be reduced by adding a donor group to form D-A-D type molecule based on the basic D-A structure. Decreased energy gap can facilitate the RISC process and promote the delayed fluorescence. Thus, the symmetric molecular structure of D-A-D is helpful for further improving the TADF feature.

Moreover, as another important factor which can influence the RISC process, the transition properties of excited states play an important role in the study of excited state properties. Natural transition orbital (NTO) analyses of S_1 and T_1 in toluene and solid phase are shown in Fig. 5. Moreover, the transition dipole moment (EDM) is gathered in Table 2. As shown in Table 2, the EDM in solid phase are bigger than in toluene, which is largely depended on that the larger overlap (S) between the highest occupied natural transition orbital (HONTO) and the

lowest unoccupied natural transition orbital (LUNTO) in solid phase than that in toluene. Thus, the overlap of natural transition orbitals is closely related to the energy gap. The overlap of PFBP-1a is 0.6001 and it becomes 0.5967 for PFBP-1b, with the corresponding ΔE_{ST} changing from 0.220 eV to 0.182 eV. Moreover, the tert-butyl substitution in donor unit can also decrease the overlap and further bring small energy gap.

The ISC and RISC rates between the singlet and triplet states are quantitatively calculated using Marcus equation are collected in Table 3. As shown in this table, PFBP-1a has an ISC rate of $5.3 \times 10^5 \text{ s}^{-1}$ and it increases to $1.2 \times 10^6 \text{ s}^{-1}$ for PFBP-1b. Similar result can also be obtained for PFBP-2a and PFBP-2b. Thus, the addition of donor unit to form D-A-D structure is easy to reduce the S_1-T_1 gap due to the enlarged orbital distribution. However, there is no obvious increase in solid phase. It is shown that the addition of a donor group in the liquid phase will increase the RISC rate and make the exciton transfer more easily and further accelerate the delayed fluorescence process. According to the Marcus equation, the ISC rate is related to SOC value, reorganization energy and adiabatic energy difference between the S_1 and T_1 states. As for organic molecules, the SOC effect is weak and corresponding value is usually smaller than 1 cm^{-1} [52,53]. However, a high ISC rate can also be achieved by small reorganization energy and energy difference between singlet and triplet states. In addition, by comparing PFBP-1a with PFBP-2a as well as PFBP-1b with PFBP-2b, it can be concluded that the ISC and RISC rates are all increased to a certain extent. So, the tert-butyl substitution in donor unit can further decrease the energy gap. As for the effect of surrounding, the ISC and RISC rates are all increased. Moreover, the relationship between temperature and reverse intersystem crossing rate is investigated, and corresponding data are shown in Fig. 6. Results show that RISC rates increase with the improvement of temperature from 100 to 300 K whether in solution or solid phase. This trend is more pronounced when the temperature changes from 100 K to 200 K than that exceeds 200 K, this confirms the TADF property. Thus, through comprehensive comparison, we propose a molecular design strategy that molecule with D-A-D structure and tert-butyl substitution in donor unit can achieve efficient TADF feature.

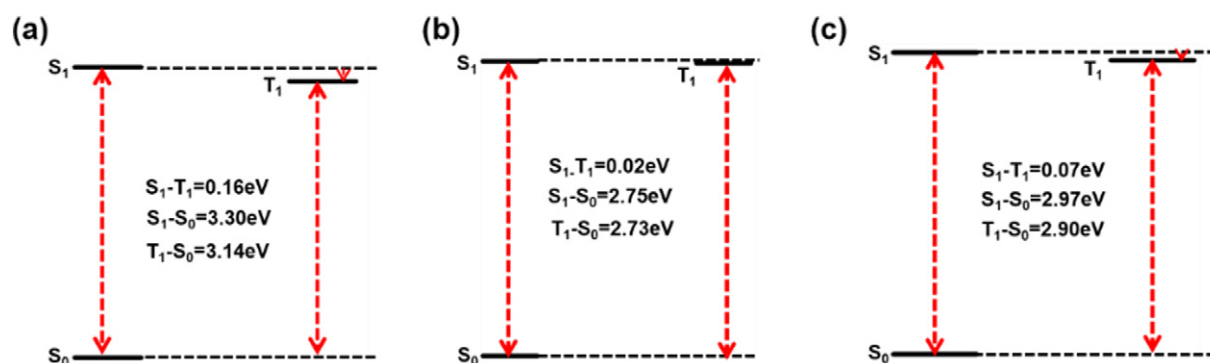


Fig. 4. Energy gap in solid phase for PFBP-1a (a), PFBP-1b (b), PFBP-2a (c).

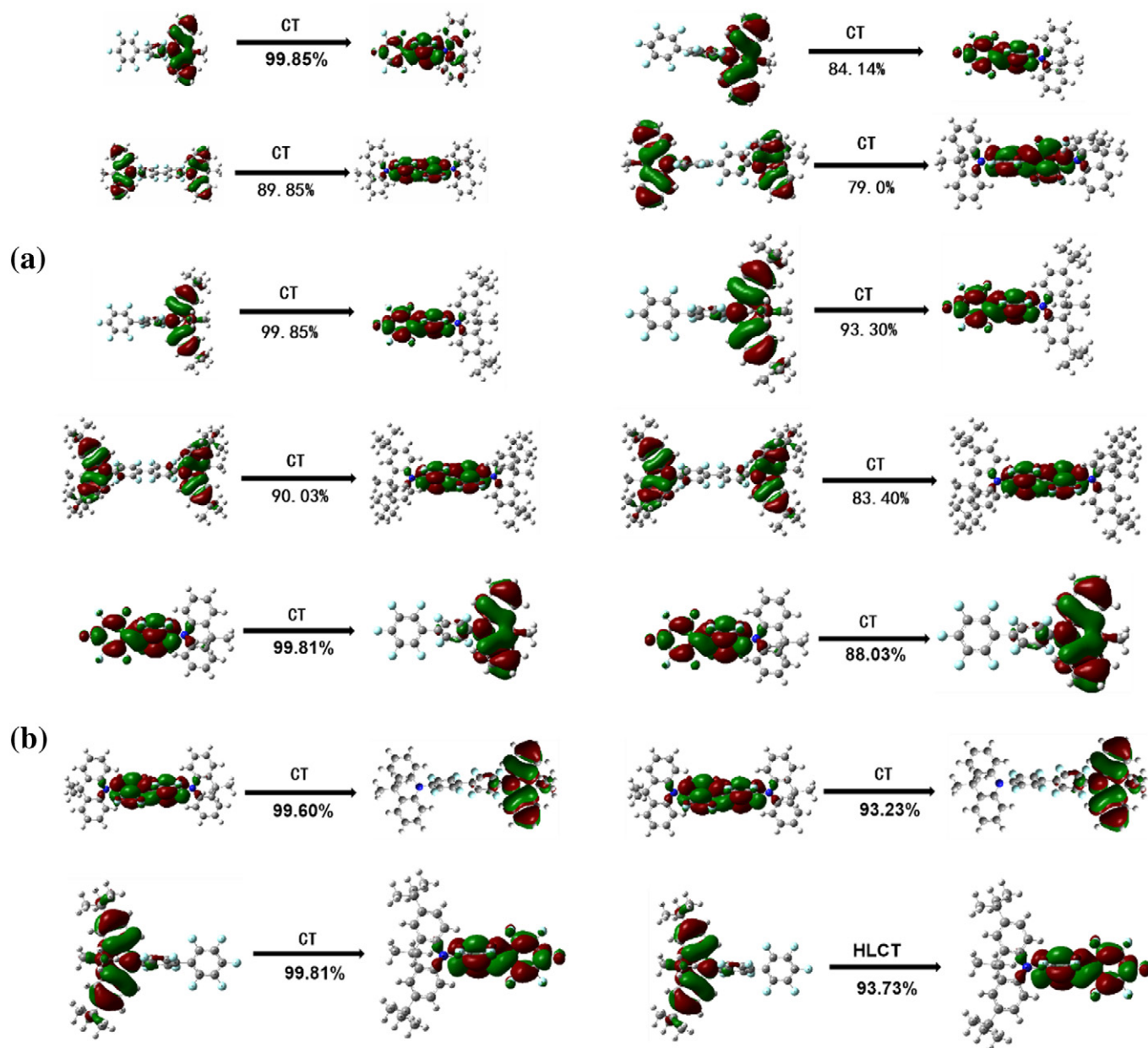


Fig. 5. Transition characteristics for S_1 and T_1 states of four molecules in toluene (a) and solid phase (b), respectively. The values under the arrows represent the ratio of NTOs of the corresponding transition.

4.2. Effect of tert-butyl substitution on luminescence properties

In this section, we compare the photophysical properties of PFBP-1a with PFBP-2a as well as PFBP-1b with PFBP-2b, and the effect of tert-butyl substitution in DMAC is also illustrated. The energy gap between S_1 and T_1 is 0.22 eV for PFBP-1a and it decreases to 0.15 eV for PFBP-

2a. Similar results can be found for PFBP-1b (0.18 eV) and PFBP-2b (0.14 eV). Thus, it can be found that the energy gap becomes smaller after substitution with tert-butyl group. As for the molecule in solid phase, the energy gap of PFBP-2a is less than PFBP-1a. It shows that the molecular structure is more stable after adding tert-butyl group. Meanwhile, as for the ISC and RISC process, not only the energy gap

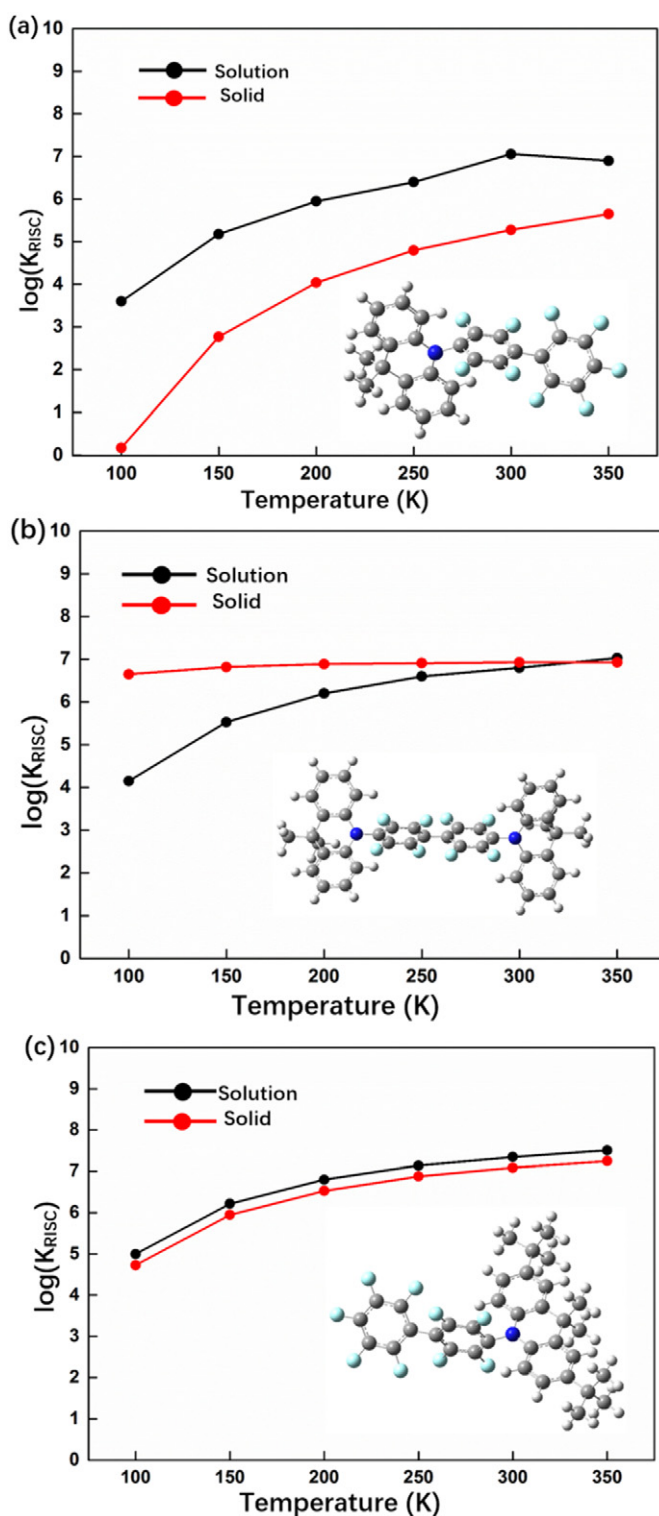
Table 2

Electric transition dipole moment (EDM), overlap (S) between HONTO and LUNTO, energy level of S_1 and T_1 as well as the S_1 - T_1 energy gap (ΔE_{ST}).

	Liquid				Solid			
	PFBP-1a	PFBP-1b	PFBP-2a	PFBP-2b	PFBP-1a	PFBP-1b	PFBP-2a	PFBP-2b
EDM	0.0359 D	0.0359 D	0.0440 D	0.1969 D	1.8119 D	0.2244 D	1.3870 D	—
S	0.6001	0.5967	0.4669	0.5000	0.5843	0.5070	0.4897	—
S_1	3.175 eV	3.137 eV	3.041 eV	3.015 eV	3.300 eV	2.745 eV	2.975 eV	—
T_1	2.955 eV	2.957 eV	2.889 eV	2.868 eV	3.140 eV	2.729 eV	2.899 eV	—
ΔE_{ST}	0.220 eV	0.182 eV	0.152 eV	0.147 eV	0.160 eV	0.016 eV	0.076 eV	—

Table 3Calculated the ISC rates from S_1 to T_1 and the RISC rates from T_1 to S_1 . (Unit s^{-1}).

	PFBP-1a		PFBP-1b		PFBP-2a		PFBP-2b	
	Toluene	Solid	Toluene	Solid	Toluene	Solid	Toluene	Solid
ISC	5.3×10^5	1.9×10^6	1.2×10^6	1.4×10^9	2.9×10^6	9.8×10^7	3.3×10^6	–
RISC	1.2×10^7	2.0×10^5	7.0×10^6	8.4×10^6	2.3×10^7	1.2×10^7	1.1×10^8	–

**Fig. 6.** Temperature dependence of RISC rates for PFBP-1a (a), PFBP-1b (b), PFBP-2a (c) in solution (black line) and solid phase (red line).

can affect it but also the spin-orbit coupling (SOC) plays an important role. Based on the quadratic response functions, the SOC constants between singlet and triplet states are calculated by Dalton 2013 package. As shown in Table 4, the SOC constant of PFBP-1a is 0.089 cm^{-1} and it changes to 0.085 cm^{-1} for PFBP-2a in toluene, while PFBP-1b is 0.072 cm^{-1} and PFBP-2b is 0.108 cm^{-1} . In solid phase, the SOC constants for PFBP-1a and PFBP-2a are 0.247 cm^{-1} and 0.312 cm^{-1} respectively. Thus, the tert-butyl substitution in DMAC unit can increase the SOC constant and further accelerate the ISC and RISC processes. Both the ISC and RISC rates as shown in Table 3 are all increased either in solution or in solid phase due to the tert-butyl substitution effect. Through the above mentioned investigations and by comparing with the structure of D-A-D configuration, the tert-butyl substitution is also an efficient way to decrease energy gap and increase SOC constant, further improving the ISC and RISC processes.

4.3. Effect of surrounding environment on luminescence properties

In this section, we compare the photophysical properties of four kind molecules in solution and solid phase and reveal the effect of surrounding environment on luminescence properties. Through analyzing the dihedral angle between donor and acceptor, we know that the rotation amplitude in solid phase is smaller than that in liquid phase. Taking PFBP-1b as an example, the configuration changes are more affected by the configuration of D-A-D than that of D-A, and there are different rotation angles in liquid phase and solid phase. The rotation angle is effectively reduced in rigid environment. The geometry changes between two states are measured by root-mean squared displacement (RMSD) with the expression of $\text{RMSD} = \sqrt{\frac{1}{N} \sum_i^{\text{natom}} [(x_i - x'_i)^2 + (y_i - y'_i)^2 + (z_i - z'_i)^2]}$ which is regarded as an effective tool to quantitatively characterize the geometric changes. These changes between S_0 and S_1 are calculated by Multiwfn [54] for all molecules both in solution and solid phase. Corresponding results are shown in Fig. 7. Results show that the RMSD for PFBP-1a in solution is 1.214 \AA , and it changes to 0.062 \AA in solid phase. As for PFBP-1b, it is 0.935 \AA in solution and decreases to 0.117 \AA in solid phase. A similar situation can also be found for PFBP-2a. Thus, due to the restricted dihedral rotation in solid phase, the RMSD values are all decreased in solid phase and this could further suppress the energy consumption process of S_1 .

In order to measure the non-radiative energy consumption, the reorganization energy and Huang-Rhys (HR) factor are further calculated using DUSHIN package [51]. $\text{HR}_k = \frac{\omega_k D_k^2}{2\hbar}$, where D_k represents the normal coordinate displacement of mode k and ω_k is the vibration

Table 4Calculated SOC constants based on S_1 ($\text{SOC}^b (\text{cm}^{-1})$) and T_1 ($\text{SOC}^c (\text{cm}^{-1})$) for four molecules in solution and solid phase.

	$\text{SOC}^b (\text{cm}^{-1})$		$\text{SOC}^c (\text{cm}^{-1})$	
	Toluene	Solid	Toluene	Solid
PFBP-1a	0.089	0.247	0.732	0.381
PFBP-1b	0.072	0.084	0.682	0.080
PFBP-2a	0.085	0.312	0.970	0.487
PFBP-2b	0.108	–	0.629	–

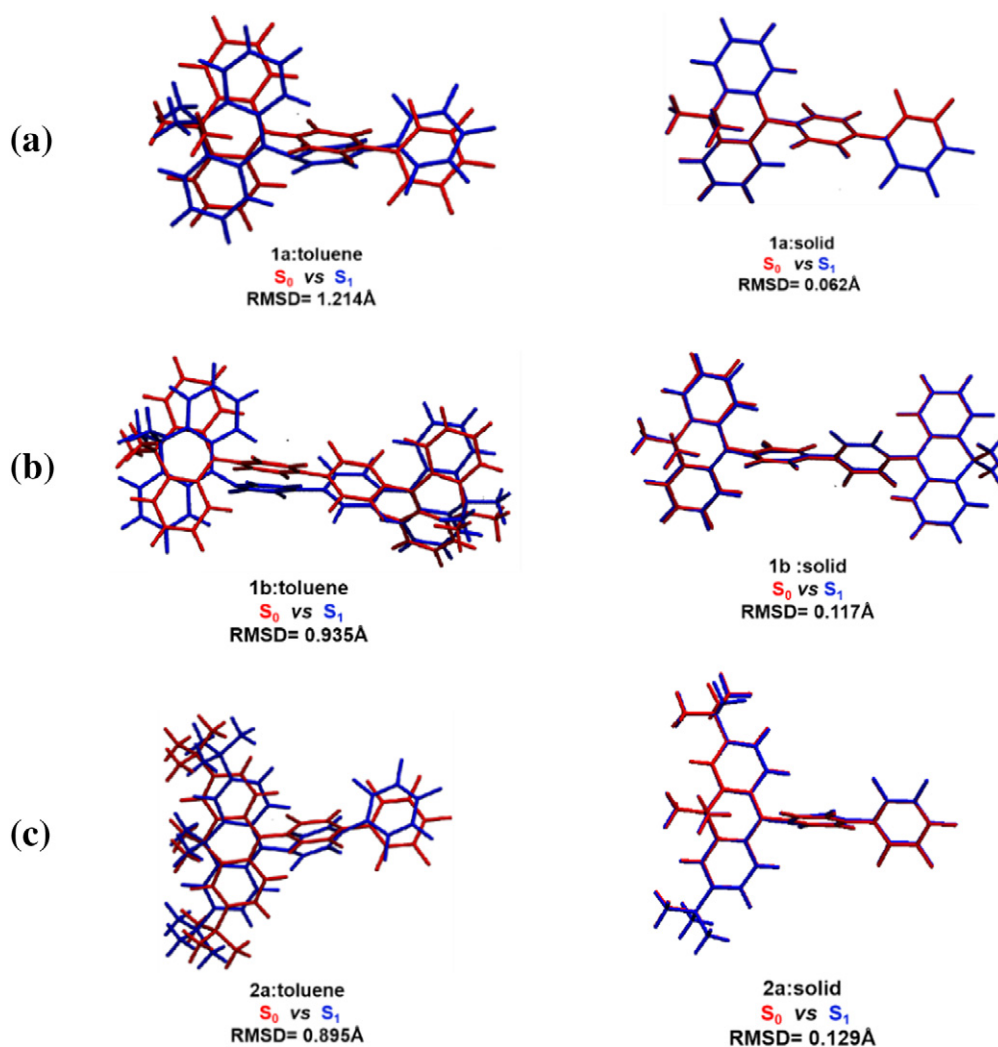


Fig. 7. Geometry changes between S_0 and S_1 in liquid and solid phase for PFBP-1a (a), PFBP-1b (b) and PFBP-2a (c).

frequency. The calculated HR factors versus the normal mode frequencies for all molecules in solution and solid phase are shown in Fig. 8. As shown in Fig. 8, the largest HR factor of PFBP-1a in the liquid phase is about 64 (565.75 cm^{-1}). While in solid phase, the largest one becomes 0.53 (62.62 cm^{-1}). As for PFBP-1b, the largest HR factor is about 93 (17.45 cm^{-1}) in liquid phase and only about 1.8 cm^{-1} in solid phase, which is obviously reduced to low frequency mode. This shows that the stronger interaction between molecules in solid phase suppresses the rotation of molecules.

Reorganization energies versus the normal-mode frequencies are displayed in Fig. 9. It is clearly shown that the reorganization energies of PFBP-1a and PFBP-1b in liquid phase are extremely larger than those in solid phase. While for the molecule in solid phase, reorganization energies both in low and high frequency modes are obviously reduced. The largest reorganization energy of PFBP-2a in liquid phase is about 3000 cm^{-1} and it is significantly decreased in solid phase. In order to further reveal the influence of molecular geometry on luminescence properties, we analyzed the reorganization energy projection in the internal coordinates of the molecule. Through analyzing the data, it is concluded that the contributions from bond length, bond angle and dihedral angle are different for molecule in solution and in solid phase. For example, the contributions of the bond length in the solid phase for PFBP-1a, PFBP-1b and PFBP-2a are 67%, 55%, 60% respectively. However, they decrease to 9%, 27%, and 29% respectively for molecule in solution. As for dihedral angle, the contributions are 87%, 88%, 66% for

PFBP-1a, PFBP-1b and PFBP-2a in solution, while for molecule in solid phase, they decrease to 17%, 31%, and 24% respectively. Thus, the reorganization in the solid phase can be significantly reduced due to the decreased contribution from dihedral angle. These results confirm that the rotation motion in low frequency regions can be effectively suppressed in solid phase, and this brings different photophysical features for molecule in solution and solid phase.

Furthermore, through analyzing the dihedral angle, RMSD value, HR factor, and reorganization energy, it can be concluded that the torsion angle is efficiently suppressed in solid phase. Thus, the non-radiative energy consumption process is hindered and the excited state energy can be released in the form of radiative transition, which subsequently brings aggregation induced emission phenomenon. Finally, we compare the difference between the ISC and RISC rates in solid phase and liquid phase. By comparing the solid phase and liquid phase environments of the three derivatives, it can be found that the ISC rate in solid phase is much higher than that in liquid phase. It is shown that the binding of the three derivatives is stronger due to the stronger interaction between the molecules in the solid phase. More excitons will transfer from the S_1 state to the T_1 state. Through comprehensive comparison, we know the ISC and RISC are all increased to a certain extent in solid phase, which is more beneficial to the occurrence of delayed fluorescence induced by aggregation. Moreover, the tert-butyl substitution in donor and D-A-D structure are all efficient ways to promote the delayed fluorescence.

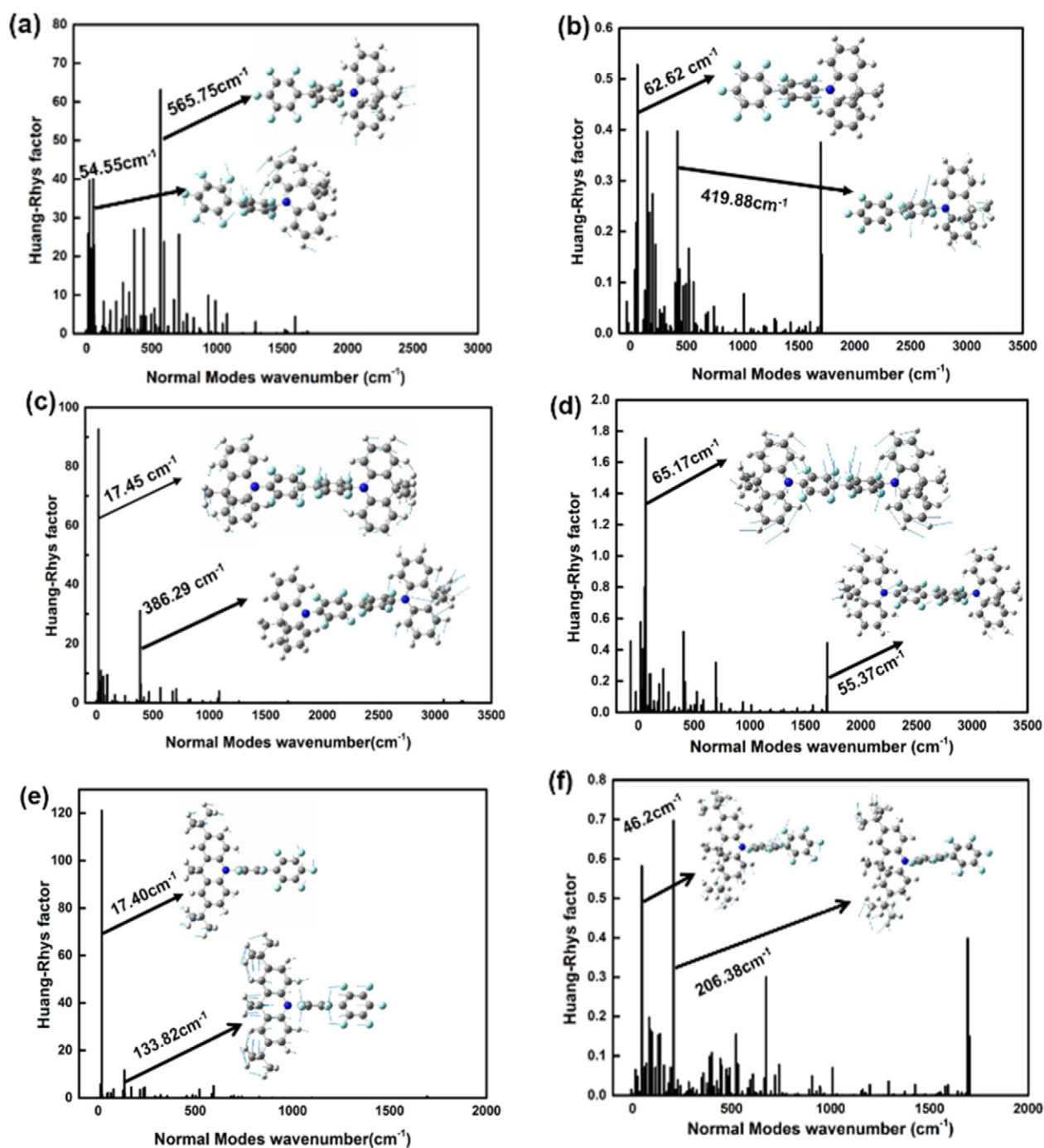


Fig. 8. HR factors versus the normal-mode frequencies of PFBP-1a (a), PFBP-1b (c), PFBP-2a (e) in toluene and PFBP-1a (b), PFBP-1b(d), PFBP-2a (f) in solid phase respectively.

5. Conclusions

The influences of D-A and D-A-D configurations, as well as the tert-butyl substitution effect on luminescence properties, are theoretically studied both in solution and solid phase. Excited states dynamics in solution and solid phase are investigated using PCM and QM/MM methods, coupled with TVCF method. The variation of geometric configuration between different states is characterized by RMSD value and geometry changes are restricted in solid phase. Moreover, the energy gap can be decreased for D-A-D configuration rather than the D-A type molecule, and tert-butyl substitution in donor unit can further promote the delayed fluorescence. In addition, the HR factor and reorganization energy are all decreased in solid phase, especially for those in low

frequency regions. Thus, non-radiative energy decay process is hindered and AIE mechanism is revealed. Furthermore, the substitution effect of tert-butyl can efficiently decrease the energy gap and increase the SOC constant, further promote the ISC and RISC rates. So a wise molecular design strategy is proposed that molecule with D-A-D structure and tert-butyl substitution can achieve efficient emitting. The present study provides reasonable explanations for experimental results and illustrates the inner AIE and TADF mechanisms.

Author contributions

Qi Lu did the most calculations and wrote the whole paper. Guanyu Jiang helped to discuss the calculation details.

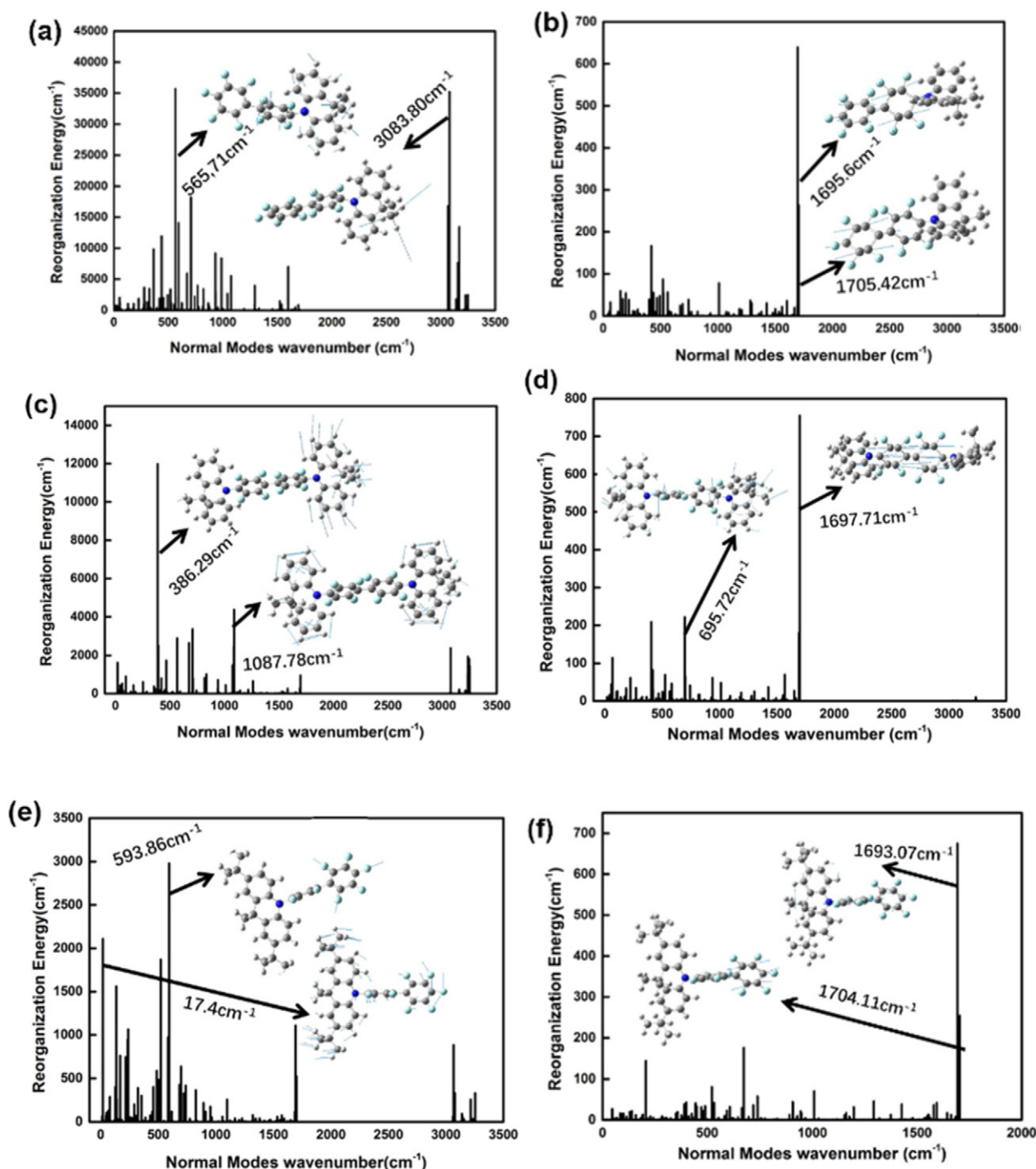


Fig. 9. Reorganization energies versus the normal-mode frequencies of PFBP-1a (a), PFBP-1b (c), PFBP-2a (e) in toluene and PFBP-1a (b), PFBP-1b (d), PFBP-2a (f) in solid phase, respectively.

Feiyan Li helped to discuss the calculation details.
 Lili Lin helped to discuss the calculation results.
 Chuan-Kui Wang helped to discuss the calculation results.
 Jianzhong Fan guided the arrangement of figures and tables.
 Yuzhi Song guided the work and revised the manuscript.

Declaration of competing interest

There are no conflicts of interest to declare.

Acknowledgements

This work is supported by the National Natural Science Foundation of China (Grant Nos. 11874241, 11904210, 11874242 and 21933002) and Shandong Provincial Natural Science Foundation, China (ZR2019MA056). Thanks to the support of Taishan Scholar Project of Shandong Province and the Scientific Research Foundation of Shandong Normal University. Thanks to the support of the Project funded by China Postdoctoral Science Foundation (Grant No. 2018M642689). Great

thanks to Professor Yi Luo, Professor Zhigang Shuai and Qian Peng for their helpful suggestions in our calculation. Thanks to Professor Yingli Niu for his great help in the usage of MOMAP.

References

- [1] H. Uoyama, K. Goushi, K. Shizu, H. Nomura, C. Adachi, Highly efficient organic light-emitting diodes from delayed fluorescence, *Nature* 492 (2012) 234–238.
- [2] I. Hladka, D. Volyniuk, O. Bezikonny, V. Kinzhyalo, T.J. Bednarchuk, Y. Danyliv, R. Lytvyn, A. Lazauskas, J.V. Grazulevicius, Polymorphism of derivatives of tert-butyl substituted acridan and perfluorobiphenyl as sky-blue OLED emitters exhibiting aggregation induced thermally activated delayed fluorescence, *J. Mater. Chem. C* 6 (2018) 13179–13189.
- [3] Y.G. Qi, J. Zhao, X. Wang, J.S. Yu, Z.G. Chi, High-efficiency phosphorescent organic light-emitting devices with low efficiency roll-off using a thermally activated delayed fluorescence material as host, *Org. Electron.* 36 (2016) 185–191.
- [4] Q. Bai, H. Liu, L. Yao, T. Shan, J. Li, Y. Gao, Z. Zhang, Y. Liu, P. Lu, B. Yang, Y. Ma, Adjusting nitrogen atom orientations of pyridine ring in tetraphenylsilane-based hosts for highly efficient blue phosphorescent organic light-emitting devices, *ACS. Appl. Mater. Inter.* 8 (2016) 24793–24802.
- [5] T. Hosokai, H. Matsuzaki, H. Nakanotani, K. Tokumaru, T. Tsutsui, A. Furube, K. Nasu, H. Nomura, M. Yahiro, C. Adachi, Evidence and mechanism of efficient thermally activated delayed fluorescence promoted by delocalized excited states, *Adv. Sci.* 3 (2017), e1603282.
- [6] C. Duan, J. Li, C. Han, D. Ding, H. Yang, Y. Wei, H. Xu, Multi-dipolar chromophores featuring phosphine oxide as joint acceptor: a new strategy toward high-efficiency blue thermally activated delayed fluorescence dyes, *Chem. Mater.* 28 (2016) 5667–5679.
- [7] L.L. Lin, Z. Wang, J.Z. Fan, C.Z. Wang, Theoretical insights on the electroluminescent mechanism of thermally activated delayed fluorescence emitters, *Org. Electron.* 41 (2017) 17–25.
- [8] J.Z. Fan, L.L. Lin, C.K. Wang, Decreasing the singlet-triplet gap for thermally activated delayed fluorescence molecules by structural modification on the donor fragment: first-principles study, *Chem. Phys. Lett.* 652 (2016) 16–21.
- [9] J.Z. Fan, S. Qiu, L.L. Lin, C.K. Wang, First-principles investigation on triazine based thermally activated delayed fluorescence emitters, *Chinese. J. Chem. Phys.* 29 (2016) 291–296.
- [10] Y. Tao, K. Yuan, T. Chen, P. Xu, H. Li, R. Chen, C. Zheng, L. Zhang, W. Huang, Thermally activated delayed fluorescence materials towards the breakthrough of organoelectronics, *Adv. Mater.* 26 (2015) 7931–7958.
- [11] C.X. Peng, J. Ding, C. Peng, P. Wang, B. Yao, J. Sun, J. Sun, L. Ran, Mechanical force-induced luminescence enhancement and chromism of a nonplanar D–A phenothiazine derivative, *J. Mater. Chem. C* 4 (2016) 5275–5280.
- [12] P. Ganesan, R. Ranganathan, Y. Chi, X.K. Liu, C.S. Lee, S.H. Liu, G.H. Lee, T.C. Lin, Y.T. Chen, P.T. Chou, Functional pyrimidine-based thermally activated delay fluorescence emitters: photophysics, mechanochromism, and fabrication of organic light-emitting diodes, *Chem. Eur. J.* 23 (2017) 2858–2866.
- [13] J. Gibson, A.P. Monkman, T.J. Penfold, The importance of vibronic coupling for efficient reverse intersystem crossing in thermally activated delayed fluorescence molecules, *Chemphyschem* 17 (2016) 2956–2961.
- [14] Z.Y. Wang, L. Ping, S. Chen, J.W.Y. Lam, Z. Wang, L. Yang, H.S. Kwok, Y. Ma, B.Z. Tang, Changing the behavior of chromophores from aggregation-caused quenching to aggregation-induced emission: development of highly efficient light emitters in the solid state, *Adv. Mater.* 22 (2010) 2159–2163.
- [15] J. Yang, A. Qin, J. Sun, B.Z. Tang, Application of AIE-active molecules in biosensing, *Chin. Sci. Bull.* 55 (2010) 1206–1213.
- [16] B.Z. Tang, X. Zhan, Y. Gui, P.P.S. Lee, Y. Liu, D. Zhu, Efficient blue emission from siloles, *J. Mater. Chem.* 11 (2001) 2974–2978.
- [17] Y. Wang, G. Zhang, M. Gao, Y. Cai, C. Zhan, Z. Zhao, D. Zhang, B.Z. Tang, Introductory lecture: recent research progress on aggregation-induced emission, *Faraday Discuss.* 196 (2016) 9–30.
- [18] L. Cai, J.Z. Fan, X.P. Kong, L.L. Lin, C.K. Wang, Luminescent properties of thermally activated delayed fluorescence molecule with intramolecular π - π interaction between donor and acceptor, *Chin. Phys. B* 26 (2017) 544–549.
- [19] Petra Galer, et al., Crystal structures and emission properties of the BF₂ complex 1-phenyl-3-(3, 5-dimethoxyphenyl)-propane-1, 3-dione: multiple chromisms, aggregation-or crystallization-induced emission, and the self-assembly effect, *J. Am. Chem. Soc.* 136 (2014) 7383.
- [20] N.A. Kukhta, D.A. da Silva Filho, D. Volyniuk, J.V. Grazulevicius, G. Sini, Can fluorone-based compounds emit in the blue region? Impact of the conjugation length and the ground-state aggregation, *Chem. Mater.* 29 (2017) 1695–1707.
- [21] R. Cammi, J. Tomasi, Remarks on the use of the apparent surface charges (ASC) methods in solvation problems: iterative versus matrix-inversion procedures and the renormalization of the apparent charges, *J. Comput. Chem.* 16 (1995) 1449–1458.
- [22] E. Cancès, B. Mennucci, J. Tomasi, A new integral equation formalism for the polarizable continuum model: theoretical background and applications to isotropic and anisotropic dielectrics, *J. Chem. Phys.* 107 (1997) 3032.
- [23] J.Z. Fan, L. Cai, L.L. Lin, C.K. Wang, Dynamics of excited states for fluorescent emitters with hybridized local and charge-transfer excited state in solid phase: a QM/MM study, *J. Phys. Chem. A* 120 (2016) 9422–9430.
- [24] B. Wang, X. Wang, W. Wang, F. Liu, Exploring the mechanism of fluorescence quenching and aggregation-induced emission of a phenylethylene derivative by QM (CASSCF and TDDFT) and ONIOM (QM:MM) calculations, *J. Phys. Chem. C* 120 (2016) 21850–21857.
- [25] G. Sun, Y. Zhao, W. Liang, Aggregation-induced emission mechanism of dimethoxy-tetraphenylethylene in water solution: molecular dynamics and QM/MM investigations, *J. Chem. Theory Comput.* 11 (2015) 2257.
- [26] J. Tomasi, B. Mennucci, R. Cammi, Quantum mechanical continuum solvation models, *J. Cheminformatics* 36 (2005) 2999–3093.
- [27] L.L. Lin, L. Cai, J.Z. Fan, C.K. Wang, Electroluminescent mechanism of thermally activated delayed fluorescence emitters: conformational effect, *J. Phys. Chem. C* 122 (2018) 19953–19961.
- [28] S.J. Strickler, R.A. Berg, Relationship between absorption intensity and fluorescence lifetime of molecules, *J. Chem. Phys.* 37 (1962) 814.
- [29] C. Angeli, C.J. Calzado, The role of the magnetic orbitals in the calculation of the magnetic coupling constants from multireference perturbation theory methods, *J. Chem. Phys.* 148 (2018), 034104.
- [30] K. Aidas, C. Angeli, K.L. Bak, V. Bakken, H. Agren, The DALTON quantum chemistry program system, *Wires. Comput. Mol. Sci.* 4 (2014) 269–284.
- [31] D.A.D. Silva Filho, V. Coropceanu, M. Lehmann, V. Lemaire, Y. Geerts, J. Piris, M.G. Debije, A.M. van de Craats, K. Senthilkumar, L.D.A. Siebbeles, Charge transport properties in discotic liquid crystals: a quantum-chemical insight into structure property relationships, *J. Am. Chem. Soc.* 126 (2004) 3271–3279.
- [32] T. Zhang, Y. Jiang, Y. Niu, D. Wang, Q. Peng, Z. Shuai, Aggregation effects on the optical emission of 1,1,2,3,4,5-hexaphenylsilole (HPS): a QM/MM study, *J. Phys. Chem. A* 118 (2014) 9094–9104.
- [33] M.I. Wang, J.Z. Fan, L.L. Lin, Influence of electron donating ability on reverse intersystem crossing rate for one kind of thermally activated delayed fluorescence molecules, *Chin. J. Chem. Phys.* 31 (2018) 291–299.
- [34] S. Sarkar, H.P. Hendrickson, D. Lee, F. DeVine, J. Jung, E. Geva, J. Kim, B.D. Dunietz, Phosphorescence in bromobenzaldehyde can be enhanced through intramolecular heavy atom effect, *J. Phys. Chem. C* 121 (2017) 3771–3777.
- [35] R.F. Chen, Y. Tang, Y. Wan, T. Chen, C. Zheng, Y. Qi, Y. Cheng, W. Huang, Promoting singlet/triplet exciton transformation in organic optoelectronic molecules: role of excited state transition configuration, *Sci. Rep.* 7 (2017) 6225.
- [36] Y.L. Niu, W. Li, Q. Peng, G. Hua, Z.G. Shuai, Molecular materials property prediction package (MOMAP) 1.0: a software package for predicting the luminescent properties and mobility of organic functional materials, *Mol. Phys.* 116 (2018) 1–13.
- [37] Z.G. Shuai, Q. Peng, Excited states structure and processes: understanding organic light-emitting diodes at the molecular level, *Phys. Rep.* 537 (2014) 123–156.
- [38] D. Escudero, Quantitative prediction of photoluminescence quantum yields of phosphors from first principles, *Chem. Sci.* 7 (2015) 1262–1267.
- [39] Q. Peng, Y. Yi, Z.G. Shuai, J. Shao, Excited state radiationless decay process with duschinsky rotation effect: formalism and implementation, *J. Chem. Phys.* 126 (2007) 1740.
- [40] Y. Niu, Q. Peng, C. Deng, X. Gao, Z.G. Shuai, Theory of excited state decays and optical spectra: application to polyatomic molecules, *J. Phys. Chem. A* 114 (2010) 7817.
- [41] L.L. Lin, J.Z. Fan, L. Cai, C.K. Wang, Excited state dynamics of new-type thermally activated delayed fluorescence emitters: theoretical view of light-emitting mechanism, *Mol. Phys.* 116 (2017) 1–10.
- [42] P.J. Stephens, F.J. Devlin, C.F. Chabalowski, M.J. Frisch, Ab initio calculation of vibrational absorption and circular Dichroism spectra using density functional force fields, *J. Phys. Chem. C* 98 (1994) 247–257.
- [43] A.D. Boese, J.M.L. Martin, Development of novel density functionals for thermochemical kinetics, *J. Chem. Phys.* 121 (2004) 3405–3416.
- [44] C. Adamo, V. Barone, Toward reliable density functional methods without adjustable parameters: the PBE0 model, *J. Chem. Phys.* 110 (1999) 6158–6159.
- [45] Y. Zhao, D.G. Truhlar, The M06 suite of density functionals for main group thermochemistry, thermochemical kinetics, noncovalent interactions, excited states, and transition elements: two new functionals and systematic testing of four M06-class functionals and 12 other, *Theor. Chem. Accounts* 120 (2008) 215–241.
- [46] G.A. Petersson, A. Bennett, T.G. Tensfeldt, M.A. Al-Laham, W.A. Shirley, J. Mantzaris, A complete basis set model chemistry. I. the total energies of closed-shell atoms and hydrides of the first-row elements, *J. Chem. Phys.* 89 (1988) 2193.
- [47] S. Lin, Q. Peng, Q. Ou, Z. Shuai, Strong solid-state fluorescence induced by restriction of the coordinate bond bending in two-coordinate copper(I)-carbene complexes, *Inorg. Chem.* 58 (2019) 14403–14409.
- [48] J.Z. Fan, Y.C. Zhang, K. Zhang, J. Liu, G.Y. Jiang, L.L. Lin, C.K. Wang, Effects of intramolecular and intermolecular interactions on excited state properties of two isomeric Cu complexes with AIE and TADF mechanisms in solid phase: a QM/MM study, *Org. Electron.* 71 (2019) 113–122.
- [49] J.Z. Fan, L.L. Lin, C.K. Wang, Excited state properties of non-doped thermally activated delayed fluorescence emitters with aggregation-induced emission: a QM/MM study, *J. Mater. WChem.* C 5 (2017) 8390–8399.
- [50] M.J. Frisch, G.W. Trucks, H.B. Schlegel, G.E. Scuseria, M.A. Robb, J.R. Cheeseman, G. Scalmani, V. Barone, G.A. Petersson, H. Nakatsuji, X. Li, M. Caricato, A.V. Marenich, J. Bloino, B.G. Janesko, R. Gomperts, B. Mennucci, H.P. Hratchian, J.V. Ortiz, A.F. Izmaylov, J.L. Sonnenberg, F.D. Williams, F. Lipparini, F. Egidi, J. Goings, B. Peng, A. Petrone, T. Henderson, D. Ranasinghe, V.G. Zakrzewski, J. Gao, N. Rega, G. Zheng, W. Liang, M. Hada, M. Ehara, K. Toyota, R. Fukuda, J. Hasegawa, M. Ishida, T. Nakajima, Y. Honda, O. Kitao, H. Nakai, T. Vreven, K. Throssell, J.A. Montgomery Jr., J.E. Peralta, F. Ogliaro, M.J. Bearpark, J.J. Heyd, E.N. Brothers, K.N. Kudin, V.N. Staroverov, T.A. Keith, R. Kobayashi, J. Normand, K. Raghavachari, A.P. Rendell, J.C. Burant, S.S. Iyengar, J. Tomasi, M. Cossi, J.M. Millam, M. Klene, C. Adamo, R. Cammi, J.W. Ochterski, R.L. Martin, K. Morokuma, O. Farkas, J.B. Foresman, D.J. Fox, Gaussian 16 Rev. a.03, Wallingford, CT 2016.
- [51] J.R. Reimers, A practical method for the use of curvilinear coordinates in calculations of normal-mode-projected displacements and duschinsky rotation matrices for large molecules, *J. Chem. Phys.* 115 (2001) 9103–9109.

- [52] X.K. Chen, B.W. Bakr, M. Auffray, Y. Tsuchiya, C.D. Sherrill, C. Adachi, J.L. Bredas, Intramolecular noncovalent interactions facilitate Thermally Activated Delayed Fluorescence (TADF), *J. Phys. Chem. Lett.* 10 (2019) 3260–3268.
- [53] Z. Chen, F. Ni, Z. Wu, Y. Hou, C. Zhong, M. Huang, G. Xie, D. Ma, C. Yang, Enhancing spin-orbit coupling by introducing a lone pair electron with p orbital character in a thermally activated delayed fluorescence emitter: photophysics and devices, *J. Phys. Chem. Lett.* 10 (2019) 2669–2675.
- [54] T. Lu, F. Chen, Multiwfn: a multifunctional wavefunction analyzer, *J. Comput. Chem.* 33 (2012) 580–592.